Comparative analysis of gyrotron backward-wave oscillators operating at different cyclotron harmonics

Y. S. Yeh
Department of Electrical Engineering, Southern Taiwan University of Technology, Tainan, Taiwan

T. H. Chang
Department of Physics, National Tsing Hua University, Hsinchu, Taiwan

T. S. Wu
Department of Electrical Engineering, Southern Taiwan University of Technology, Tainan, Taiwan

A comparative analysis between the fundamental and second cyclotron harmonics of gyrotron backward-wave oscillators (gyro-BWOs) is presented. The simulation results reveal that nonlinear field contraction is a common feature for both harmonic interactions. Besides, the electron transit angle, used to characterize the axial modes of the fundamental harmonic TE_{11} mode at the start-oscillation conditions, is found to be applicable even for the second harmonic TE_{21} mode. Each axial mode of either the fundamental harmonic TE_{11} or the second harmonic TE_{21} modes is maintained at a constant value of the electron transit angle while changing the operating parameters, such as magnetic field and beam voltage. Extensive numerical calculations are conducted for the start-oscillation currents and tuning properties. Moreover, single-mode operating regimes are suggested where the second harmonic TE_{21} gyro-BWO could generate a considerable output power, comparing with the fundamental harmonic TE_{11} gyro-BWO. © *2004 American Institute of Physics.* [DOI: 10.1063/1.1783314]

I. INTRODUCTION

The high power capability of gyrotrons makes them attractive sources in the millimeter wave range.[1–4] The gyrotron backward-wave oscillator (gyro-BWO) is a promising source of coherent millimeter-wave radiation based on the electron cyclotron maser instability on a backward waveguide mode. The most appealing characteristic of the gyro-BWO is that its frequency can be tuned by adjusting either the magnetic field or the beam voltage, or both. Theoretical studies of the gyro-BWO first appeared in the mid-1960s in Soviet literature.[5] Linear theory has been developed to analyze the start-oscillation conditions of the gyro-BWO.[6–8] However, the efficiency of the gyro-BWO is lower than that of other gyrotron devices for uniform waveguide structure.[9]

Tapering the magnetic field has been found to significantly improve the efficiency of the gyro-BWO.[10,11] Besides, a tapered interaction structure has been proposed and employed experimentally. The output power twice as high as that of the uniform tube structure has been reported.[12–14] A nonlinear self-consistent method has been employed to investigate the nonlinear behavior of the gyro-BWO with a tapered magnetic field and waveguide wall radius.[5] The maximum efficiency of the gyro-BWO with tapering was improved to be almost three times higher than that of the gyro-BWO without tapering. On the other hand, the injection locking technique has also been demonstrated to support phase control and spectral purity of a gyro-BWO.[15] However, the need for a high magnetic field limits its applicability as a millimeter-wave source.

Researches have attempted to alleviate the high magnetic field requirements in harmonic operation.[16–19] The harmonic operation of the gyrotron has been widely used in gyromonotrons, gyroklystron amplifiers, and gyrotron traveling wave amplifiers (gyro-TWTs). In gyrodevices, the electrons interact resonantly with the electromagnetic wave under the synchronism condition,

$$\omega - k_z v_z - s\Omega_c \gtrsim 0, \tag{1}$$

where ω is the wave frequency, k_z is the propagation constant, v_z is the electron axial velocity, s is the cyclotron harmonic number, and Ω_c is the relativistic electron cyclotron frequency. The magnetic field is proportional to the relativistic electron cyclotron frequency, so the magnetic field of a gyrotron operating at the sth cyclotron harmonic is nearly $1/s$ of that of a gyrotron operating at the fundamental cyclotron harmonic. Because of the weak beam-wave interaction, the gyrotron operating at harmonic cyclotron was found to produce higher power with improved stability.[16–19]

This study compares the fundamental harmonic TE_{11} and second harmonic TE_{21} gyro-BWOs. The field profiles at various interaction lengths are analyzed to elucidate the saturated behavior of the gyro-BWOs. The spurious oscillations may compete with the operating mode in the gyro-BWO, and thus the start-oscillation conditions of the transverse modes (TE_{mn} modes) are examined. The high-order axial modes ($\ell > 1$) of the gyro-BWOs may oscillate where the beam currents exceed the start-oscillation currents of the modes. The electron transit angles of the axial modes are also considered. Moreover, the ability to tune the output power and oscillation frequency by adjusting the magnetic field and beam voltage is discussed.

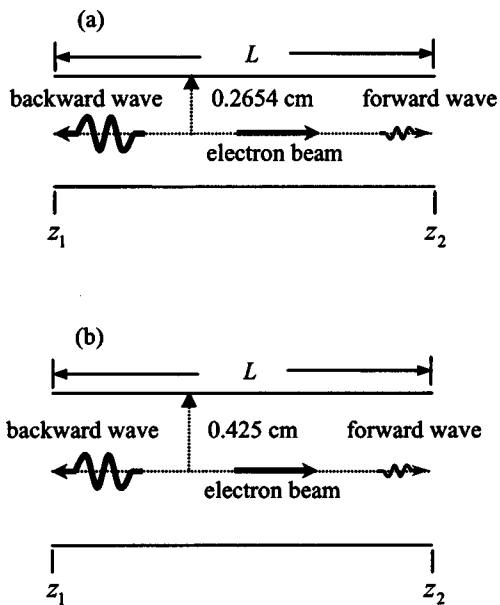This study employs a nonlinear self-consistent code to

4547

FIG. 1. Schematic drawings of (a) the fundamental harmonic TE_{11} and (b) the second harmonic TE_{21} gyro-BWOs.

FIG. 2. $\omega-k_z$ diagrams of the transverse waveguide modes and the cyclotron harmonic beam-wave resonance lines in (a) the fundamental harmonic TE_{11} and (b) the second harmonic TE_{21} gyro-BWOs.

analyze the gyro-BWOs. This single-mode nonlinear code is based on the commonly used technique of steady-state particle tracking in a weakly nonuniform interaction structure. The code works for both gyro-TWTs and gyro-BWOs by setting different boundary conditions.[19–24] The correctness and validity of the nonlinear code was demonstrated experimentally.[21,22] The rest of this paper is organized as follows. Section II presents the numerical method and the simulation model. Section III presents the results obtained for the fundamental and second harmonic gyro-BWOs, including saturated behavior, start-oscillation conditions of the transverse modes and the axial modes, output power and oscillation frequency tuning range. Section IV draws conclusions.

II. NUMERICAL METHOD AND SIMULATION MODEL

A nonlinear self-consistent code, based on a slow time scale formulation, was developed to evaluate the performance of stable gyro-TWT amplifiers[19–21] and gyro-BWOs.[22–24] The electron beam interacting with a single waveguide mode (TE_{mn}) is presumed. Thus the structural nonuniformity must be sufficiently weak to prevent mode conversion.

The field equation driven by a current source can be expressed as[21]

$$\left(\frac{d^2}{dz^2}+k_z^2\right)f(z)=i\frac{8|I_b|}{x_{mn}^2 K_{mn}\omega}\sum_{j=1}^{N}W_j\frac{\mathbf{v}_j(z)\cdot\mathbf{E}*(r_j,\theta_j,t_j,z)}{v_{zj}(z)f*(z)},$$
(2)

where $f(z)$ is the field profile function along the axis, I_b is the beam current, x_{mn} is the nth root of the derivative of Bessel function $J'_m(x)$, $\mathbf{E}*$ is the complex conjugate of $\mathbf{E}$, W_j is a normalized weighting factor for the jth electron, $\mathbf{v}_j$ is the velocity for the jth electron, v_{zj} is the axial velocity for the
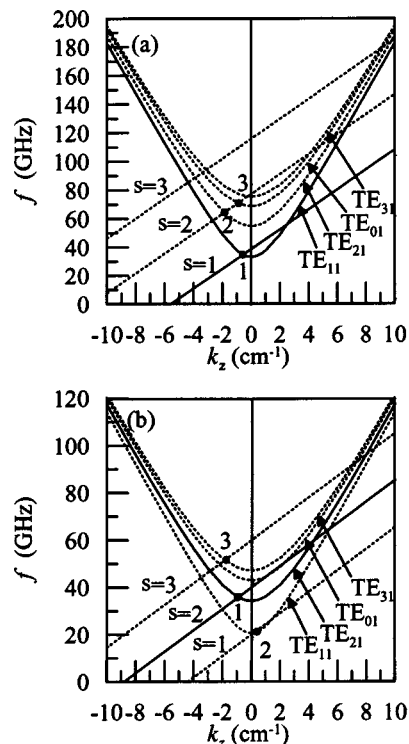
jth electron, and the transverse coordinates r_j and θ_j and the time coordinate t_j are functions of z for the jth electron. The terms k_z and K_{mn} are given in

$$k_z^2=\frac{1}{c^2}\left\{\omega^2-\omega_{cmn}^2\left[1-(1+i)\frac{\delta}{r_w}\left(1+\frac{m^2}{x_{mn}^2-m^2}\frac{\omega^2}{\omega_{cmn}^2}\right)\right]\right\},$$
(3)

and

$$K_{mn}=J_{mn}^2(x_{mn})\left(1-\frac{m^2}{x_{mn}^2}\right),$$
(4)

where $\omega_{cmn}=x_{mn}c/r_w$ is the cutoff frequency and δ is the skin depth.

A pure backward wave is present at the left end ($z=z_1$), and a pure forward wave is present at the right end ($z=z_2$) in a gyro-BWO, as shown in Fig. 1. Accordingly, the boundary conditions at the ends are[21]

$$f'(z_1)=-ik_zf(z_1),$$
(5a)

$$f'(z_2)=ik_zf(z_2),$$
(5b)

where k_z is the propagation constant in the input/output waveguide.

A Ka-band fundamental harmonic TE_{11} gyro-BWO was conducted at National Tsing Hua University (NTHU).[22] The beam parameters were beam voltage $V_b=100$ kV, perpendicular-to-parallel velocity ratio $\alpha=1.0$, and guiding center radius $r_c=0.09$ cm. This study modeled the gyro-BWO circuit as a uniform waveguide [Fig. 1(a)] to prevent complications associated with the nonuniform
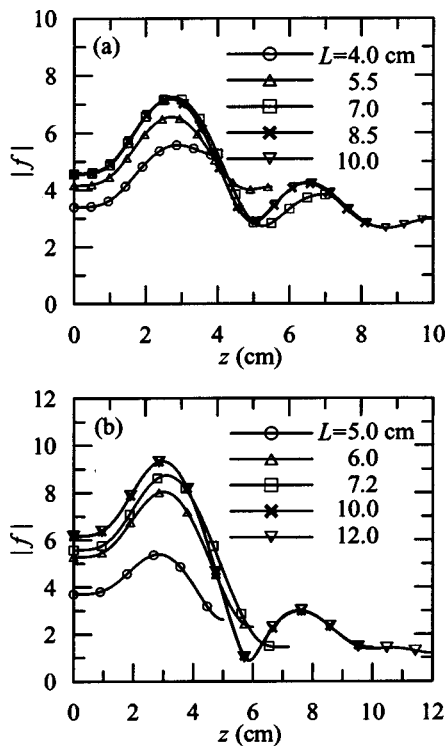
FIG. 3. Field profiles of (a) the fundamental harmonic TE_{11} and (b) the second harmonic TE_{21} gyro-BWOs at the fundamental axial mode ($\ell=1$) for the different interaction lengths. In (a) $V_b=100$ kV, $I_b=2.5$ A, $B_0=13.7$ kG, $\alpha=1.0$, $r_c=0.09$ cm, $\Delta v_z/v_z=5\%$, and $r_w=0.2654$ cm. In (b) $V_b=120$ kV, $I_b=12$ A, $B_0=7.6$ kG, $\alpha=1.05$, $r_c=0.155$ cm, $\Delta v_z/v_z=8\%$, and $r_w=0.425$ cm.

FIG. 4. Start-oscillation current I_{st} vs magnetic field B_0 for the different transverse modes in (a) the fundamental harmonic TE_{11} and (b) the second harmonic TE_{21} gyro-BWOs. In (a) $V_b=100$ kV, $L=5.5$ cm, $\alpha=1.0$, $r_c=0.09$ cm, $\Delta v_z/v_z=5\%$, and $r_w=0.2654$ cm. In (b) $V_b=120$ kV, $L=7.2$ cm, $\alpha=1.05$, $r_c=0.155$ cm, $\Delta v_z/v_z=8\%$, and $r_w=0.425$ cm.

waveguide.[25,26] The uniform waveguide is cylindrical with a radius r_w of 0.2654 cm. Figure 2(a) plots the $\omega-k_z$ diagram of the transverse waveguide modes and the cyclotron harmonic beam-wave resonance lines. The operating mode is shown by an intersection in which the fundamental harmonic cyclotron beam-wave resonance lines ($s=1$) grazes the TE_{11} mode [point 1 in Fig. 2(a)]. On the other hand, a second harmonic TE_{21} gyro-BWO with uniform waveguide structure is shown in Fig. 1(b). The parameters of the gyro-BWO are $V_b=120$ kV, $\alpha=1.05$, $r_c=0.155$ cm, and $r_w=0.425$ cm. Figure 2(b) shows the $\omega-k_z$ diagram of the gyro-BWO. The intersection in the backward region [point 1 in Fig. 2(b)] is the operating mode in which the second harmonic cyclotron beam-wave resonance line ($s=2$) grazes the TE_{21} mode. The other intersections [points 2 and 3 in Fig. 2(b)] are potential sources of oscillations.

To accurately determine the interaction efficiency of the gyro-BWO, the axial velocity spread $\Delta v_z/v_z$ of the electron gun for the gyro-BWO is included in the calculations. Using a simulation code,[27,28] the axial velocity spread of an optimal magnetron injection gun (MIG) for the fundamental harmonic TE_{11} gyro-BWO is less than 5% when the beam current is 2.5 A. The weak beam-wave interaction in the second harmonic TE_{21} gyro-BWO allows much higher operating beam current. The axial velocity spread of a MIG for the second harmonic TE_{21} gyro-BWO is less than 8% when the beam current is 12 A. Therefore, the axial velocity spreads associated with the fundamental harmonic TE_{11} and second
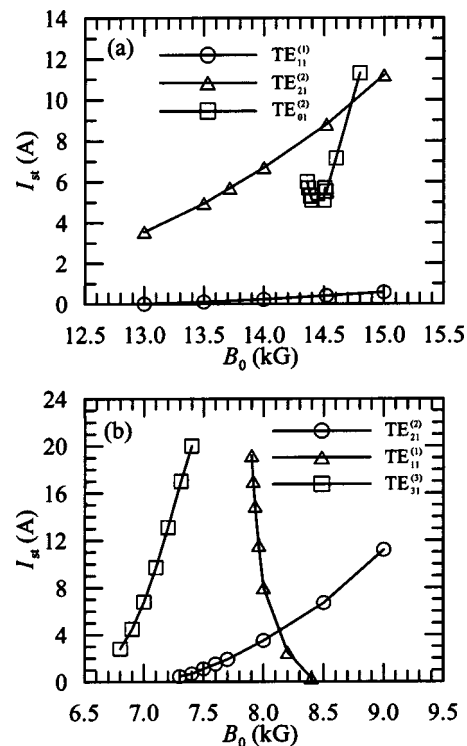
harmonic TE_{21} gyro-BWOs are here assumed to be 5% and 8%, respectively.

III. RESULTS AND DISCUSSION

A. Nonlinear field contraction

Figure 3(a) displays the field profiles of the fundamental harmonic TE_{11} gyro-BWO for a fixed beam current of 2.5 A. The simulated results show that the peak field amplitude increases with interaction length until the length reaches a certain value, called the relaxation length. The results are consistent with the results of Ref. 23. Since the bulk field is concentrated at the beam entrance due to backward-wave interaction, the spent electron beam with greater velocity spread barely contributes to the field. Therefore, the interaction length of the gyro-BWO need not be more than the relaxation length. Figure 3(b) plots the field profiles of the second harmonic TE_{21} gyro-BWO for a fixed beam current of 12 A. The simulated results indicate that any length beyond the relaxation length adds slightly to the peak field amplitude in the gyro-BWO. For uniform waveguide structure, the relaxation lengths of the fundamental harmonic TE_{11} and second harmonic TE_{21} gyro-BWOs are around 7 and 10 cm, respectively.

Previous investigations also showed that the operation of a gyro-BWO might enter a nonstationary state at long interaction lengths or high beam currents.[24] Moreover, the competing transverse and axial modes occur easily at long interaction lengths or high beam currents. Thus the interaction
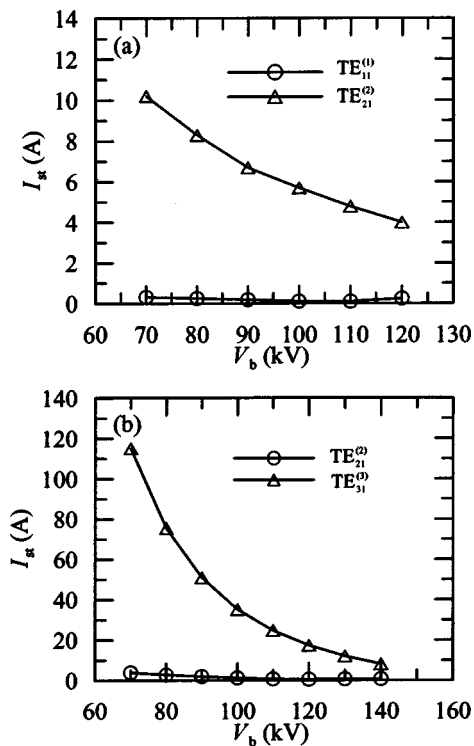
FIG. 5. Start-oscillation current I_{st} vs beam voltage V_b for the different transverse modes in (a) the fundamental harmonic TE_{11} and (b) the second harmonic TE_{21} gyro-BWOs. In (a) $B_0=13.7$ kG, $L=5.5$ cm, $\alpha=1.0$, $r_c=0.09$ cm, $\Delta v_z/v_z=5\%$, and $r_w=0.2654$ cm. In (b) $B_0=7.3$ kG, $L=7.2$ cm, $\alpha=1.05$, $r_c=0.155$ cm, $\Delta v_z/v_z=8\%$, and $r_w=0.425$ cm.

FIG. 6. Start-oscillation current I_{st} vs magnetic field B_0 for the different axial modes in (a) the fundamental harmonic TE_{11} and (b) the second harmonic TE_{21} gyro-BWOs. The parameters are the same as in Fig. 4.

lengths of the gyro-BWOs should be devised as short as possible to prevent them from entering nonstationary states and exhibiting spurious oscillations. Hence, the interaction lengths of the fundamental harmonic TE_{11} and second harmonic TE_{21} gyro-BWOs are assumed to be 5.5 and 7.2 cm, respectively, in the following calculations.

B. Start-oscillation conditions of various transverse modes

The competing transverse modes must be eluded in order to achieve a stable, single-mode operation of a gyro-BWO. The fundamental harmonic TE_{11} gyro-BWO is most susceptible to the $TE_{21}^{(2)}$ and $TE_{01}^{(2)}$ modes (the superscript refers to the cyclotron harmonic number) [points 2 and 3 in Fig. 2(a)]. Figure 4(a) plots the start-oscillation current as a function of the magnetic field. The simulated results indicate that the start-oscillation currents of the $TE_{21}^{(2)}$ mode declined with declining magnetic field. Meanwhile, the start-oscillation currents of the $TE_{01}^{(2)}$ mode have minimum at 14.4 kG. This may occur because the start-oscillation currents of the spurious oscillations ($TE_{21}^{(2)}$ and $TE_{01}^{(2)}$ modes) are decreased significantly when the oscillations become absolute instabilities near the cutoff points in the interaction waveguide [Fig. 2(a)].

On the other hand, the $TE_{11}^{(1)}$ and $TE_{31}^{(3)}$ modes [points 2 and 3 in Fig. 2(b)] may take place in the second harmonic TE_{21} gyro-BWO. Figure 4(b) plots the start-oscillation current as a function of the magnetic field. The simulated results
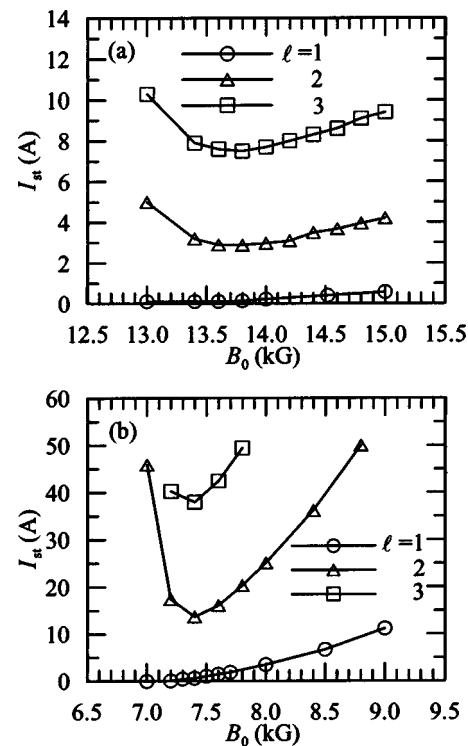
also reveal that the start-oscillation currents of the spurious oscillations ($TE_{11}^{(1)}$ and $TE_{31}^{(3)}$ modes) in the second harmonic TE_{21} gyro-BWO are decreased significantly when the oscillation frequencies are close to the cutoff frequencies in the waveguide [Fig. 2(b)]. Meanwhile, the magnetic field is between 7.2 and 7.9 kG to tune the frequency of the stable gyro-BWO when the beam current is 12 A [Fig. 4(b)]. Below and beyond this limit, the oscillation could be unstable due to possible multimode competition.

Figures 5(a) and 5(b) show the start-oscillation current of the oscillation in various transverse modes as a function of the beam voltage in the fundamental harmonic TE_{11} and second harmonic TE_{21} gyro-BWOs, respectively. The simulated results indicate that the start-oscillation currents of the $TE_{21}^{(2)}$ mode declined as the beam voltage increased in the fundamental harmonic TE_{11} gyro-BWO [Fig. 5(a)]. Also, the oscillation at high beam voltage becomes absolute instability near the cutoff frequency of the interaction waveguide [Fig. 2(a)]. Because of much high start-oscillation current at the magnetic field of 13.7 kG [Fig. 4(a)], the $TE_{01}^{(2)}$ mode is not shown in Fig. 5(a). Similarly, the points of intersection of the TE_{31} mode and the third harmonic cyclotron beam-wave resonance line ($s=3$) approached the cutoff point of the waveguide as the beam voltage increased in the second harmonic TE_{21} gyro-BWO [Fig. 2(b)]. Thus the start-oscillation currents of the $TE_{31}^{(3)}$ mode declined as the beam voltage increased in the gyro-BWO [Fig. 5(b)]. The $TE_{11}^{(1)}$ mode is not shown in Fig. 5(b), due to much high start-oscillation current at the magnetic field of 7.3 kG [Fig. 4(b)].
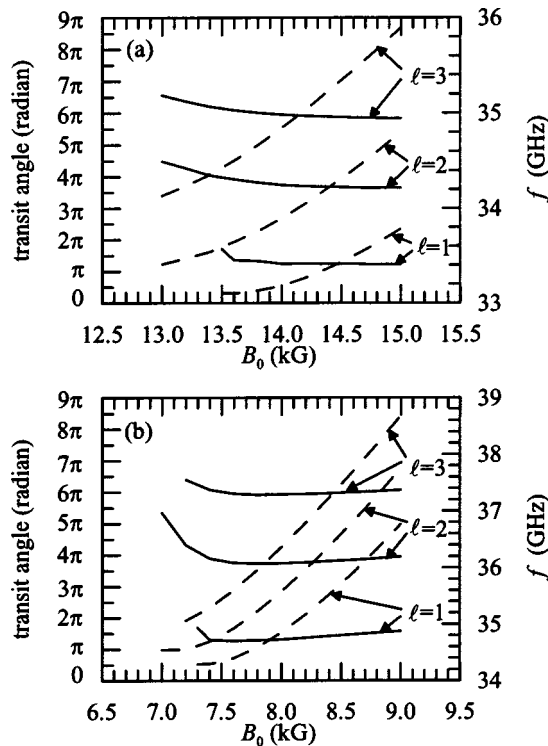
FIG. 7. Transit angle (unbroken curves) and start-oscillation frequency f (dashed curves) vs magnetic field B_0 for the different axial modes in (a) the fundamental harmonic TE_{11} and (b) the second harmonic TE_{21} gyro-BWOs. The parameters are the same as in Fig. 4.
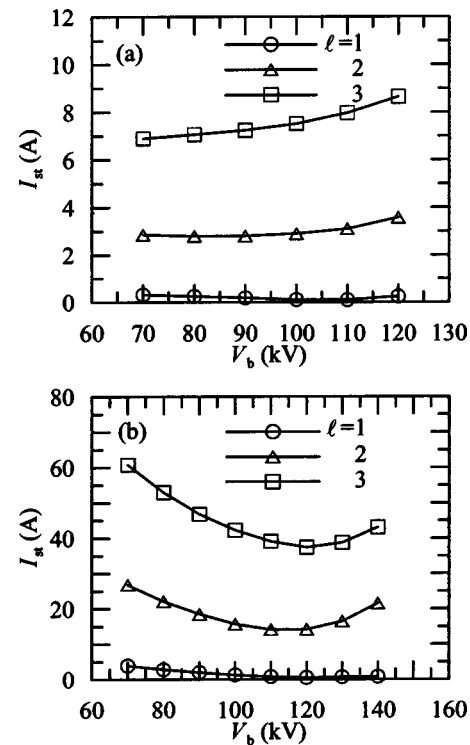
FIG. 8. Start-oscillation current I_{st} vs beam voltage V_b for the different axial modes in (a) the fundamental harmonic TE_{11} and (b) the second harmonic TE_{21} gyro-BWOs. The parameters are the same as in Fig. 5.

C. Electron transit angles of the axial modes

Given a resonator, the superposition of reflected waves at both ends results in the axial field profile of a cold mode. The gyro-BWO, formed by the internal feedback consisting of the forward-moving electron beam and the backward-propagating wave, with a uniform waveguide structure does not have cold modes, unlike the gyromonotron. The axial mode of the gyro-BWO depends totally on the dynamics of the beam-wave interaction.[23] The high-order axial modes ($\ell > 1$) may compete with the operating mode when the beam currents exceed the start-oscillation currents of the high-order modes. Figure 6(a) shows that the three lowest order axial modes of the fundamental harmonic TE_{11} gyro-BWO are obtained for different magnetic fields. The simulated results indicate that the higher order axial modes always require higher start-oscillation currents, independently of the magnetic field. The results are consistent with the cited investigation.[24] Meanwhile, the minimum start-oscillation current of the high-order axial modes in the gyro-BWO is 2.9 A [Fig. 6(a)].

The electron transit angle provides the total phase variation of the backward wave as experienced by the electrons in the interaction space. The electron transit angle is defined as[24]

$$\Theta = (\omega - k_z v_{z0} - s\Omega_c)(L/v_{z0}), \qquad (6)$$

where v_{z0} is the initial axial velocity of the electron. Figure 7(a) plots the electron transit angle and start-oscillation frequency as functions of the magnetic field in the fundamental

harmonic TE_{11} gyro-BWO. The cited study[24] has shown that the output wave power and deposited beam power balance each other at a minimum beam current where the axial mode has the same electron transit angle. The start-oscillation currents, electron transit angles, and start-oscillation frequencies of the second harmonic TE_{21} gyro-BWO are similar to those of the fundamental harmonic TE_{11} gyro-BWO, as shown in Figs. 6(b) and 7(b). The results indicate that the minimum start-oscillation current of the high-order axial modes in the second harmonic TE_{21} gyro-BWO is 13.7 A [Fig. 6(b)]. Meanwhile, each axial mode of the gyro-BWO is characterized by the constancy of the electron transit angle when the mode operates in a high magnetic field ($B_0 > 7.5$ kG) [Fig. 7(b)].

Figure 8 plots the start-oscillation currents of the lowest order axial modes as functions of the beam voltages. The simulated results reveal that the start-oscillation current increases with the axial mode number, independently of the beam voltage, in the fundamental harmonic TE_{11} and the second harmonic TE_{21} gyro-BWOs. Figure 9 plots the electron transit angle and start-oscillation frequency as functions of the beam voltage in the gyro-BWOs. The simulated results indicate that the electron transit angles of the fundamental harmonic TE_{11} and second harmonic TE_{21} gyro-BWOs are almost constant when the gyro-BWOs operate at low beam voltages. However, the axial modes have high electron transit angles when gyro-BWOs are operated at low magnetic fields or high beam voltages (Figs. 7 and 9), perhaps because
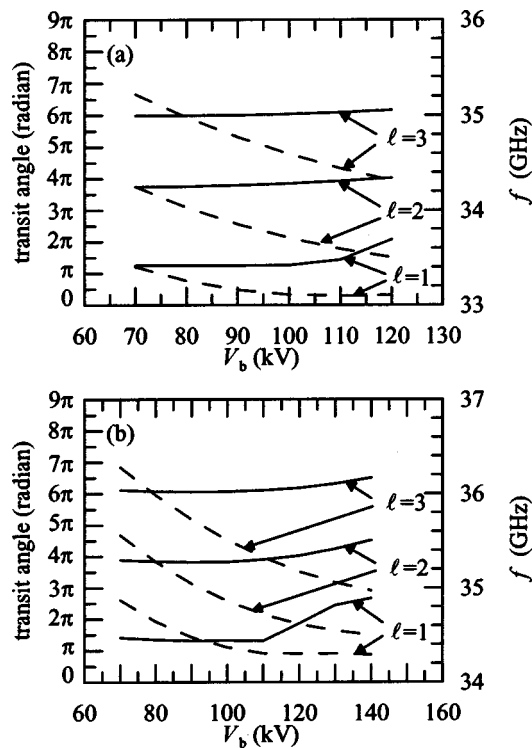
FIG. 9. Transit angle (unbroken curves) and start-oscillation frequency f (dashed curves) vs beam voltage V_b for the different axial modes in (a) the fundamental harmonic TE_{11} and (b) the second harmonic TE_{21} gyro-BWOs. The parameters are the same as in Fig. 5.

FIG. 10. Output power P_{out} (unbroken curves) and oscillation frequency f (dashed curves) vs magnetic field B_0 for the different beam currents in (a) the fundamental harmonic TE_{11} and (b) the second harmonic TE_{21} gyro-BWOs. The parameters are the same as in Fig. 4.

the oscillations at low magnetic fields or high beam voltages become absolute instabilities near the cutoff points in the interaction waveguide.

D. Performance of the gyro-BWOs

Figure 10 plots the variation of the output power and oscillation frequency at various beam currents as functions of the magnetic field. The simulated results show that the maximum output power of the stable fundamental harmonic TE_{11} gyro-BWO is only about 30 kW at a beam current of 2.5 A [Fig. 10(a)]. If the beam current of the gyro-BWO is increased to 5 A, the maximum output power is added to 59 kW. Similarly, the maximum output power is added to 64 kW at a beam voltage of 115 kV where the beam current is increased to 5 A [Fig. 11(a)].

Because of much weak beam-wave coupling in the harmonic interaction, the operating beam current of the second harmonic TE_{21} gyro-BWO requires a high value, 12 A. At this current value, stable operating magnetic field ranges from 7.2 to 7.9 kG, see Fig. 4(b). The maximum output power of the stable gyro-BWO is about 137 kW when the beam current is 12 A [Fig. 10(b)]. If the beam current of the gyro-BWO is increased to 15 A, the maximum output power is added to 180 kW. Similarly, the maximum output power of the gyro-BWO is added to 183 kW at a beam voltage of 125 kV where the beam current is increased to 15 A [Fig. 11(b)].
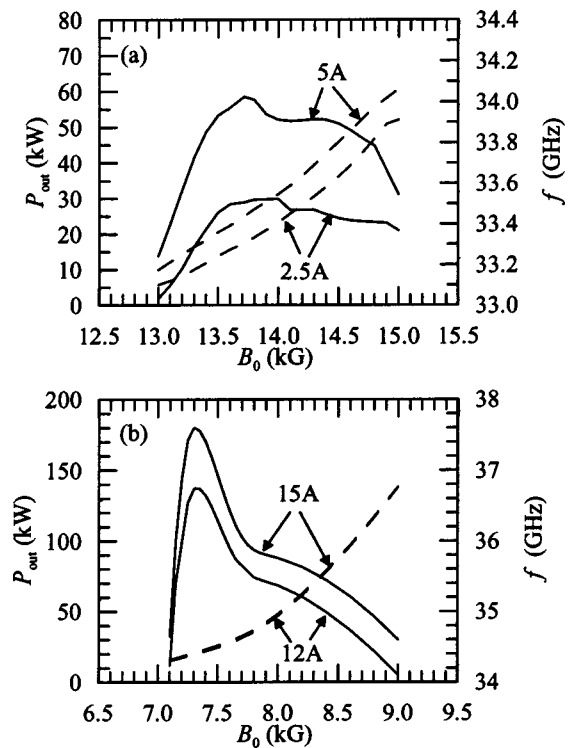
IV. CONCLUSIONS

A comparative analysis of the fundamental harmonic TE_{11} and the second harmonic TE_{21} gyro-BWOs was performed by a nonlinear self-consistent code. In both harmonic interactions, any length beyond the relaxation length adds slightly to the peak field amplitude. Meanwhile, the electron transit angle of each axial mode has a unique value, almost independent of the magnetic field and beam voltage, unless the oscillation frequency closes to the waveguide cutoff.

Both operating beam currents of the fundamental harmonic TE_{11} and second harmonic TE_{21} gyro-BWOs were shown to be restricted by not only the competing transverse modes but also the high-order axial modes. The fundamental harmonic TE_{11} gyro-BWO is most susceptible to the $TE_{21}^{(2)}$ and $TE_{01}^{(2)}$ modes. The frequency tuning range of the second harmonic TE_{21} gyro-BWO is limited by the $TE_{11}^{(1)}$ and $TE_{31}^{(3)}$ modes. The high-order axial modes of both gyro-BWOs generally require high start-oscillation currents, independently of the magnetic field or beam voltage. The minimum start-oscillation currents of the competing modes in the fundamental harmonic TE_{11} and second harmonic TE_{21} gyro-BWOs are 2.9 and 13.7 A, respectively. Compared with the fundamental harmonic TE_{11} gyro-BWO, the beam current and output power of the stable second harmonic TE_{21} gyro-BWO are added to 12 A and 137 kW, respectively.

The competing transverse and axial modes are composed of the major limitation on the beam current for stable operations. The distributed wall losses technique[21,29] could be applied to suppress the spurious oscillations. The present re-
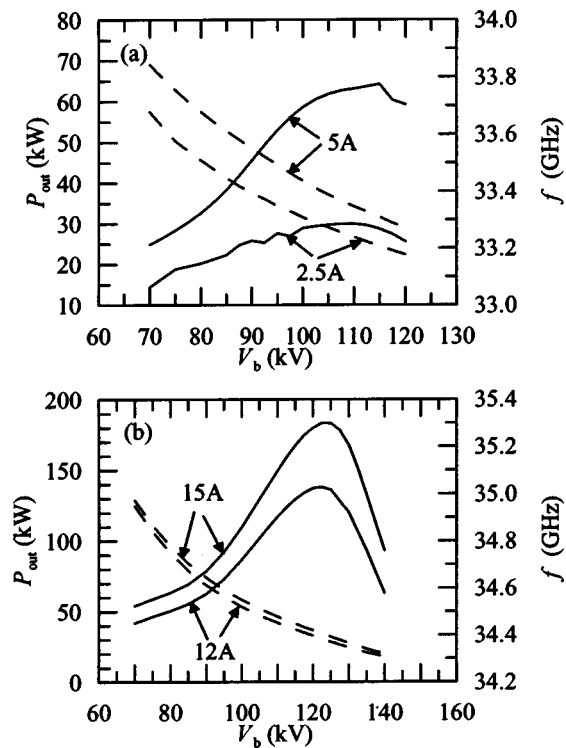
Phys. Plasmas, Vol. 11, No. 10, October 2004

Comparative analysis of gyrotron backward-wave…   4553

FIG. 11. Output power P_{out} (unbroken curves) and oscillation frequency f (dashed curves) vs beam voltage V_b for the different beam currents in (a) the fundamental harmonic TE_{11} and (b) the second harmonic TE_{21} gyro-BWOs. The parameters are the same as in Fig. 5.

sults clarify some characteristics of the harmonic interaction of a gyro-BWO. To the practical interest, however, the efficiency and tuning bandwidth should be further optimized. The gyro-BWO may exhibit self-modulation behavior while displaying no evidence of mode competition, and thus multimode time-dependent codes[24–26] should be carried out for an in-depth stability study. The nonstationary behavior of the gyro-BWO may not only change the efficiency and tuning bandwidth, but also may affect the stability operation.

ACKNOWLEDGMENTS

[1] J. L. Seftor, V. L. Granatstein, K. R. Chu, P. Sprangle, and M. E. Read, IEEE J. Quantum Electron. **15**, 848 (1979).
[2] L. R. Barnett, Y. Y. Lau, K. R. Chu, and V. L. Granatstein, IEEE Trans. Electron Devices **28**, 872 (1981).
[3] R. S. Symons, H. R. Jory, S. J. Hegji, and P. E. Ferguson, IEEE Trans. Microwave Theory Tech. **29**, 181 (1981).
[4] D. S. Furuno, D. B. Mcdermott, C. S. Kou, N. C. Luhmann, Jr., and P. Vitello, Phys. Rev. Lett. **62**, 1314 (1989).
[5] G. S. Nusinovich and O. Dumbrajs, IEEE Trans. Plasma Sci. **24**, 620 (1996).
[6] J. M. Wachtel and E. J. Wachtel, Appl. Phys. Lett. **37**, 1059 (1980).
[7] S. Y. Park, V. L. Granatstein, and R. K. Parker, Int. J. Electron. **57**, 1109 (1984).
[8] C. S. Kou, Phys. Plasmas **1**, 3093 (1994).
[9] S. Y. Park, R. H. Kyser, C. M. Armstrong, R. K. Parker, and V. L. Granatstein, IEEE Trans. Plasma Sci. **18**, 321 (1990).
[10] A. K. Ganguly and S. Ahn, Int. J. Electron. **67**, 261 (1989).
[11] A. T. Lin, Phys. Rev. A **46**, R4516 (1992).
[12] M. T. Walter, R. M. Gilgenbach, P. R. Menge, and T. A. Spencer, IEEE Trans. Plasma Sci. **22**, 578 (1994).
[13] C. S. Kou, C. H. Chen, and T. J. Wu, Phys. Rev. E **57**, 7162 (1998).
[14] M. T. Walter, R. M. Gilgenbach, J. W. Luginsland, J. M. Hochman, J. I. Rintamaki, R. L. Jaynes, Y. Y. Lau, and T. A. Spencer, IEEE Trans. Plasma Sci. **24**, 636 (1996).
[15] C. S. Kou, S. H. Chen, L. R. Barnett, H. Y. Chen, and K. R. Chu, Phys. Rev. Lett. **70**, 924 (1993).
[16] A. T. Lin, K. R. Chu, C. C. Lin, C. S. Kou, D. B. McDermott, and N. C. Luhmann, Jr., Int. J. Electron. **72**, 873 (1992).
[17] Q. S. Wang, C. S. Kou, D. B. McDermott, A. T. Lin, K. R. Chu, and N. C. Luhmann, Jr., IEEE Trans. Plasma Sci. **20**, 163 (1992).
[18] Q. S. Wang, D. B. McDermott, and N. C. Luhmann, Jr., Phys. Rev. Lett. **75**, 4322 (1995).
[19] Y. S. Yeh, C. L. Hung, C. W. Su, T. S. Wu, Y. Y. Shin, and Y. T. Lo, Int. J. Infrared Millim. Waves **25**, 29 (2004).
[20] K. R. Chu, H. Y. Chen, C. L. Hung, T. H. Chang, L. R. Barnett, S. H. Chen, and T. T. Yang, Phys. Rev. Lett. **81**, 4760 (1998).
[21] K. R. Chu, H. Y. Chen, C. L. Hung, T. H. Chang, L. R. Barnett, S. H. Chen, T. T. Yang, and D. Dialetis, IEEE Trans. Plasma Sci. **27**, 391 (1999).
[22] T. H. Chang, S. H. Chen, L. R. Barnett, and K. R. Chu, Phys. Rev. Lett. **87**, 064802 (2001).
[23] S. H. Chen, K. R. Chu, and T. H. Chang, Phys. Rev. Lett. **85**, 2633 (2000).
[24] S. H. Chen, T. H. Chang, K. F. Pao, C. T. Fan, and K. R. Chu, Phys. Rev. Lett. **89**, 268303 (2002).
[25] G. S. Nusinovich, A. N. Vlasov, and T. M. Antonsen, Jr., Phys. Rev. Lett. **87**, 218301 (2001).
[26] A. Grudiev and K. Schünemann, IEEE Trans. Plasma Sci. **30**, 851 (2002).
[27] Y. S. Yeh, M. H. Tsao, H. Y. Chen, and T. H. Chang, Int. J. Infrared Millim. Waves **21**, 1397 (2000).
[28] Y. S. Yeh, T. H. Chang, and C. T. Fan, Int. J. Infrared Millim. Waves **22**, 983 (2001).
[29] Y. S. Yeh, T. S. Wu, Y. T. Lo, C. W. Su, and S. C. Wu, Int. J. Electron. **90**, 517 (2003).